A High Performance Pneumatic Force Actuator System: Part I—Nonlinear Mathematical Model

Article *in* Journal of Dynamic Systems Measurement and Control · September 2000

DOI: 10.1115/1.1286336

2 authors:

Edmond Richer
Southern Methodist University
70 PUBLICATIONS **1,735** CITATIONS

SEE PROFILE

Yildirim Hurmuzlu
Southern Methodist University
80 PUBLICATIONS **3,045** CITATIONS

SEE PROFILE

A High Performance Pneumatic Force Actuator System: Part I—Nonlinear Mathematical Model

Edmond Richer[1]

Yildirim Hurmuzlu

Southern Methodist University,
School of Engineering and Applied Science,
Mechanical Engineering Department,
Dallas, TX 75275

In this paper, we developed a detailed mathematical model of dual action pneumatic actuators controlled with proportional spool valves. Effects of nonlinear flow through the valve, air compressibility in cylinder chambers, leakage between chambers, end of stroke inactive volume, and time delay and attenuation in the pneumatic lines were carefully considered. We performed system identification, numerical simulation, and model validation experiments for two types of air cylinders and different connecting tubes length. The mathematical model of the present article is used in a sequel article to develop high performance nonlinear pneumatic force controllers. [S0022-0434(00)00503-7]

1 Introduction

Modern force-reflecting teleoperation, haptic interfaces, and other applications in robotics require high performance force actuators, with high force output per unit weight. It is also important to have linear, fast and accurate response, as well as low friction and mechanical impedance. Traditional geared electrical motors cannot provide these characteristics. Few newly designed motors have special direct-drive actuators, with no intermediate mechanisms. Yet, applications such as teleoperation master arms with gravitational compensation, require long duration, static high force output. In these cases, direct drive electrical actuators necessitate special cooling systems to dissipate the excessive heat.

We believe that pneumatic cylinders can offer a better alternative to electrical or hydraulic actuators for certain types of applications. Pneumatic actuators provide the previously enumerated qualities at low cost. They are also suitable for clean environments and safer and easier to work with. However, position and force control of these actuators in applications that require high bandwidth is somehow difficult. This is mainly due to compressibility of air and highly nonlinear flow through pneumatic system components. In addition, design and space considerations in many applications force the command valve to be positioned at relatively large distance from the pneumatic cylinder. Thus, the effects of time delay and attenuation caused by the connecting tubes becomes significant. These difficulties limited the early use of pneumatic actuators to simple applications that required only positioning at the two ends of the stroke. Subsequently, more complete mathematical models for the thermodynamic and flow equations in the charging-discharging processes were developed (Shearer [1]). As a result, more complex position controllers, based on the linearization around the mid stroke position were developed (Burrows [2], Liu and Bobrow [3]). These simplified models provided only modest performance improvements. During the last decade, nonlinear control techniques were implemented using digital computers. Bobrow and Jabbari [4] and McDonell and Bobrow [5] used adaptive control for force actuation and trajectory tracking, applied to an air powered robot. Improved results were presented, but they were confined mainly for low frequencies (approx. 1 Hz). Sliding mode position controllers were also tested (Arun et al. [6], Tang and Walker [7]), again with improved results at low frequencies. As a general characteristic, the mathematical models used in these controllers assumed no piston seals friction, linear flow through the valve, and neglected the valve dynamics. Ben-Dov and Salcudean [8] developed a forced-controlled pneumatic actuator that provided a force with an amplitude of 2 N at 16 Hz. Their model included the valve dynamics and the nonlinear characteristics of the compressible flow through the valve. A comparison between linear and nonlinear controllers applied to a rotary pneumatic actuator is presented by Richard and Scavarda [9]. The mathematical model accounted for the leakage between actuator's chambers and the nonlinear variation of the valve effective area with the applied voltage. Their model depends heavily on curve fitting using experimental values, making it difficult to apply to even slightly different systems.

The goal of this article is to provide an accurate model of a pneumatic actuator system controlled by a proportional spool valve. This model is targeted to develop force controllers that perform at significantly more demanding operating conditions. For this purpose, the model takes into consideration the friction in the piston seals, the difference in active areas of the piston due to the rod, inactive volume at the ends of the piston stroke, leakage between chambers, valve dynamics and flow nonlinearities through the valve orifice, and time delay and flow amplitude attenuation in valve-cylinder connecting tubes. Since the ultimate purpose of the modeling effort is for control applications, the proposed equations should be suitable for on-line implementation.

We designed special experiments in order to identify the unknown characteristics of the pneumatic system, such as: valve discharge coefficient, valve spool viscous friction coefficient, and piston friction forces. The model was finally tested using two experiments that allowed the measurement of the actuator force output and piston displacement. The experimental results were compared with the results obtained by numerical simulation.

2 System Dynamics

A typical pneumatic system includes a force element (the pneumatic cylinder), a command device (valve), connecting tubes, and position, pressure and force sensors. The external load consists of the mass of external mechanical elements connected to the piston and perhaps a force produced by an environmental interaction. A schematic representation of the pneumatic actuator system is shown in Fig. 1, with variables of interest specified for each component.

[1]Presently with Advanced Radiological Sciences in the University of Texas Southwestern Medical Center at Dallas.

Contributed by the Dynamic Systems and Control Division for publication in the JOURNAL OF DYNAMIC SYSTEMS, MEASUREMENT, AND CONTROL. Manuscript received by the Dynamic Systems and Control Division June 23, 1999. Associate Technical Editor: S. Nair.

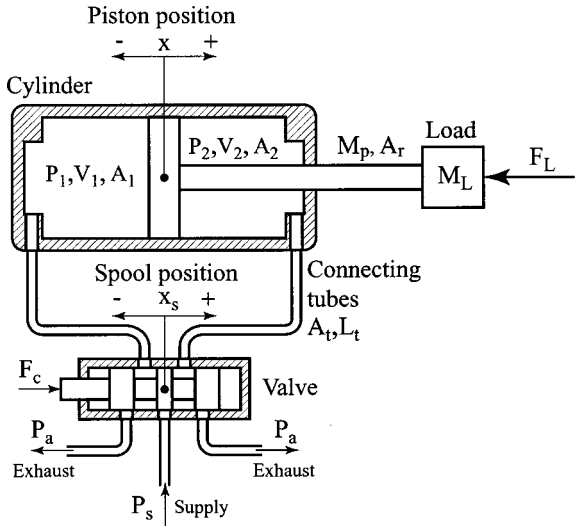

Fig. 1 Schematic representation of the pneumatic cylinder-valve system

2.1 Piston-Load Dynamics. The equation of motion for the piston-rod-load assembly can be expressed as

$$(M_L+M_p)\ddot{x}+\beta\dot{x}+F_f+F_L=P_1A_1-P_2A_2-P_aA_r \qquad (1)$$

where M_L is the external load mass, M_p is the piston and rod assembly mass, x is the piston position, β is the viscous friction coefficient, F_f is the Coulomb friction force, F_L is the external force, P_1 and P_2 are the absolute pressures in actuator's chambers, P_a is the absolute ambient pressure, A_1 and A_2 are the piston effective areas, and A_r is the rod cross-sectional area. The right-hand side of Eq. (1) represents the actuator active force, produced by the pressure differential acting across the piston. In order to control the actuator force output, one has to finely tune the pressure levels in the cylinder chambers using the command element (the pneumatic valve). This requires detailed models for the dynamics of pressure in both chambers of the actuator, valve dynamics, and connecting tubes.

2.2 Model of the Cylinder Chambers. In this section we seek to develop a differential equation that links the chamber pressures to the mass flow rate through the system and piston translational speed. In previous works (see Liu and Bobrow [3], Ben-Dov and Salcudean [8]; Richard and Scavarda [9]) the authors derived this equation using the assumption that the charging and discharging processes were both adiabatic. Al-Ibrahim and Otis [10] found experimentally that the temperature inside the chambers lays between the theoretical adiabatic and isothermal curves. The experimental values of the temperature were close to the adiabatic curve only for the charging process. For the discharging of the chamber the isothermal assumption was closer to the measured values. In this article we derive the pressure dynamics equation in a way that accounts for the different thermal characteristics of the charging and discharging processes of the cylinder chambers.

The most general model for a volume of gas consists of three equations (see Hullender and Woods [11]): an equation of state (ideal gas law), the conservation of mass (continuity) equation, and the energy equation. Assuming that: (i) the gas is perfect, (ii) the pressures and temperature within each chamber are homogeneous, and (iii) kinetic and potential energy terms are negligible, these equations can be written for each chamber. Considering the control volume V, with density ρ, mass m, pressure P, and temperature T, the ideal gas law can be written as

$$P=\rho RT \qquad (2)$$

where, R is the ideal gas constant. Using the continuity equation the mass flow rate can be expressed as

$$\dot{m}=\frac{d}{dt}(\rho V) \qquad (3)$$

which can be also expressed as

$$\dot{m}_{\text{in}}-\dot{m}_{\text{out}}=\dot{\rho}V+\rho\dot{V} \qquad (4)$$

where, $\dot{m}_{\text{in}}$ and $\dot{m}_{\text{out}}$ are the mass flows entering and leaving the chamber.
The energy equation can be written as follows

$$q_{\text{in}}-q_{\text{out}}+kC_v(\dot{m}_{\text{in}}T_{\text{in}}-\dot{m}_{\text{out}}T)-\dot{W}=\dot{U} \qquad (5)$$

where q_{in} and q_{out} are the heat transfer terms, k is the specific heat ratio, C_v is the specific heat at constant volume, T_{in} is the temperature of the incoming gas flow, $\dot{W}$ is the rate of change in the work, and $\dot{U}$ is the change of internal energy. The total change in internal energy is

$$\dot{U}=\frac{d}{dt}(C_vmT)=\frac{1}{k-1}\frac{d}{dt}(PV)=\frac{1}{k-1}(V\dot{P}+P\dot{V}) \qquad (6)$$

in which we used the ideal gas relation, $C_v=R/(k-1)$. Now, substituting $\dot{W}=P\dot{V}$ and Eq. (6), into Eq. (5)

$$q_{\text{in}}-q_{\text{out}}+\frac{k}{k-1}\frac{P}{\rho T}(\dot{m}_{\text{in}}T_{\text{in}}-\dot{m}_{\text{out}}T)-\frac{k}{k-1}P\dot{V}=\frac{1}{k-1}V\dot{P} \qquad (7)$$

Assuming that the incoming flow is already at the temperature of the gas in the chamber considered for analysis, the energy equation becomes

$$\frac{k-1}{k}(q_{\text{in}}-q_{\text{out}})+\frac{1}{\rho}(\dot{m}_{\text{in}}-\dot{m}_{\text{out}})-\dot{V}=\frac{V}{kP}\dot{P} \qquad (8)$$

Further simplification can be made by analyzing the heat transfer terms in Eq. (8). If the process is considered to be adiabatic $(q_{\text{in}}-q_{\text{out}}=0)$, the time derivative of the chamber pressure is

$$\dot{P}=k\frac{P}{\rho V}(\dot{m}_{\text{in}}-\dot{m}_{\text{out}})-k\frac{P}{V}\dot{V} \qquad (9)$$

or, substituting ρ from Eq. (2)

$$\dot{P}=k\frac{RT}{V}(\dot{m}_{\text{in}}-\dot{m}_{\text{out}})-k\frac{P}{V}\dot{V} \qquad (10)$$

If the process is considered to be isothermal (T=constant), then the change in internal energy is

$$\dot{U}=C_v\dot{m}T \qquad (11)$$

and Eq. (8) can be written as

$$q_{\text{in}}-q_{\text{out}}=P\dot{V}-\frac{P}{\rho}(\dot{m}_{\text{in}}-\dot{m}_{\text{out}}) \qquad (12)$$

Then, the rate of change in pressure will be

$$\dot{P}=\frac{RT}{V}(\dot{m}_{\text{in}}-\dot{m}_{\text{out}})-\frac{P}{V}\dot{V} \qquad (13)$$

A comparison of Eqs. (10) and (13) shows that the only difference is the specific heat ratio term k. Thus, both equations can be written as

$$\dot{P}=\frac{RT}{V}(\alpha_{\text{in}}\dot{m}_{\text{in}}-\alpha_{\text{out}}\dot{m}_{\text{out}})-\alpha\frac{P}{V}\dot{V} \qquad (14)$$

with α, α_{in}, and α_{out} taking values between 1 and k, depending on the actual heat transfer during the process. In Eq. (14) one does not have to know the exact heat transfer characteristics, but merely estimate the coefficients α, α_{in}, and α_{out}. The fact that the

uncertainty of the estimation is bounded by $k-1$ is also very important from the control design perspective. For the charging process, a value of α_{in} close to k is recommended, while for the discharging of the chamber α_{out} should be chosen close to 1. The thermal characteristic of compression/expansion process due to the piston movement is better described using $\alpha=1.2$ (see Al-Ibrahim and Otis [10]).

Choosing the origin of piston displacement at the middle of the stroke, the volume of each chamber can be expressed as

$$V_i = V_{0i} + A_i\left(\frac{1}{2}L \pm x\right) \tag{15}$$

where $i=1,2$ is the cylinder chambers index, V_{0i} is the inactive volume at the end of stroke and admission ports, A_i is the piston effective area, L is the piston stroke, and x is the piston position. The difference between the piston effective areas for each chamber A_1 and A_2 is due to the piston rod. Substituting Eq. (15) into (14), the time derivative for the pressure in the pneumatic cylinder chambers becomes

$$\dot{P}_i = \frac{RT}{V_{0i} + A_i\left(\frac{1}{2}L \pm x\right)}(\alpha_{in}\dot{m}_{in} - \alpha_{out}\dot{m}_{out}) - \alpha\frac{PA_i}{V_{0i} + A_i\left(\frac{1}{2}L \pm x\right)}\dot{x} \tag{16}$$

In this new form, the pressure equation accounts for the different heat transfer characteristics of the charging and discharging processes, air compression or expansion due to piston movement, the difference in effective area on the opposite sides of the piston, and the inactive volume at the end of stroke and admission ports. There are two sources for the flow entering a cylinder chamber: (a) the pressure tank, through the pneumatic valve and connecting tube, (b) the neighboring chamber if it has a higher pressure and piston seals are leaking. The air can flow out to the atmosphere through the valve or piston rod seals, or to the second chamber if it has a smaller pressure. The leakage between the chambers can be neglected for regular pneumatic cylinders with rubber type seals, but can be significant for low friction cylinders that have graphite or Teflon seals. The expressions for the input and output flows will be derived in the next section.

2.3 Model of Valve-Cylinder Connecting Tube. The tubes that connect the valve with the actuator have two effects on the system response. First, the pressure drop along the tube will induce a decrease in the steady-state air flow through the valve. Second, the flow profile at the outlet will be delayed with respect to the one at the inlet by the time increment necessary for the acoustic wave to travel through the entire length of the tube. This will affect the transient response of the flow in the cylinder chambers. The problem of the pressure losses and time delay in long pneumatic lines was analyzed by many authors: Schuder and Binder [12], Hougen et al. [13], Andersen [14], Whitmore et al. [15], Elmadbouly and Abdulsadek [16]. Most of these investigators assumed fully developed laminar flow through the tube. They provide infinite series solutions for the pressure dynamics, or approximate the response to harmonic pressure inputs using a second order linear system.

Because we model for online control applications, in our derivation we seek a simpler expression for the mass flow through the tube. The expression should not require intensive computation like the series solution and should not increase the order of the system as the second-order linear approximation does. We also extend the analysis to include wholly turbulent flow.

In Schuder and Binder [12] and Andersen [14] the two basic equations governing the flow in a circular pneumatic line were derived as

$$\frac{\partial P}{\partial s} = -R_t u - \rho\frac{\partial u}{\partial t} \tag{17}$$

$$\frac{\partial u}{\partial s} = -\frac{1}{\rho c^2}\frac{\partial P}{\partial t} \tag{18}$$

where P is the pressure along the tube, u is the velocity, ρ is the air density, c is the sound speed, s is the tube axis coordinate, and R_t is the tube resistance. Introducing the mass flow through the tube as $\dot{m}_t = \rho A_t u$, where A_t is the tube cross-sectional area

$$\frac{\partial P}{\partial s} = -\frac{1}{A_t}\frac{\partial \dot{m}_t}{\partial t} - \frac{R_t}{\rho A_t}\dot{m}_t \tag{19}$$

$$\frac{\partial \dot{m}_t}{\partial s} = -\frac{A_t}{c^2}\frac{\partial P}{\partial t} \tag{20}$$

These equations are similar to those in Elmadbouly and Abdulsadek [16] except for the second term in Eq. (19) that accounts for resistance of the tube. Differentiating Eq. (19) with respect with t and Eq. (20) with respect to s, we obtain the equation for the mass flow through the tube as

$$\frac{\partial^2 \dot{m}_t}{\partial t^2} - c^2\frac{\partial^2 \dot{m}_t}{\partial s^2} + \frac{R_t}{\rho}\frac{\partial \dot{m}_t}{\partial t} = 0 \tag{21}$$

This equation represents a generalization of a wave equation, with an additional dissipative term. The proposed mass flow equation can be solved by using the following form (see Chester [17])

$$\dot{m}_t(s,t) = \phi(t)v(s,t) \tag{22}$$

where $v(s,t)$ and $\phi(t)$ are new unknown functions. Substituting Eq. (22) into (21) yields

$$\phi\frac{\partial^2 v}{\partial t^2} - c^2\phi\frac{\partial^2 v}{\partial s^2} + \left(\phi\frac{R_t}{\rho} + 2\phi'\right)\frac{\partial v}{\partial t} + \left(\phi'\frac{R_t}{\rho} + \phi''\right)v = 0 \tag{23}$$

In order to simplify the equation for v, we determine $\phi(t)$ such that, after substitution in Eq. (23), the remaining equation in v contains no first derivative term (Chester [17]),

$$2\phi' + \phi\frac{R_t}{\rho} = 0 \tag{24}$$

which is equivalent to,

$$\phi(t) = e^{-(R_t/2\rho)t} \tag{25}$$

The resulting equation for v will be,

$$\frac{\partial^2 v}{\partial t^2} - c^2\phi\frac{\partial^2 v}{\partial s^2} + \frac{R_t^2}{4\rho^2}v = 0 \tag{26}$$

which is a *dispersive hyperbolic equation*. Chester [17] showed that Eq. (26) had a solution in the form of a progressive wave that propagates along the tube with any constant velocity different than c. The fact that the solution waves do not propagate with the same velocity is called *dispersion*, and it is caused by the term $(R_t/2\rho)^2 v$. The tubes under consideration are not sufficiently long to cause appreciable dispersion (they are in the range of 1 to 2 m, compared to 10–100 meters), so we assumed that the dispersion is small, and can be neglected. This assumption yields,

$$\frac{\partial^2 v}{\partial t^2} - c^2\phi\frac{\partial^2 v}{\partial s^2} = 0 \tag{27}$$

This is the classic one-dimensional wave equation, and can be solved for specific boundary and initial conditions. We assume that there is no flow through the tube at $t=0$, the flow at the inlet $(s=0)$ is an arbitrary time dependent function $h(t)$, and there is no reflection from the end connected at the pneumatic cylinder. The corresponding initial and boundary conditions become,

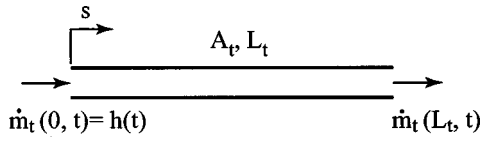

Fig. 2 Pneumatic tube notations

$$\begin{cases} v(s,0)=0 \\ \dfrac{\partial v}{\partial t}(s,0)=0 \\ v(0,t)=h(t) \end{cases} \tag{28}$$

The solution for this boundary-initial-value problem is (see Chester [17])

$$v(s,t)=\begin{cases} 0 & \text{if } t<s/c \\ h\left(t-\dfrac{s}{c}\right) & \text{if } t>s/c \end{cases} \tag{29}$$

The input wave will reach the end of the tube in a time period $\tau = L_t/c$. Replacing t by L_t/c in Eq. (25), and substituting ρ from the equation of state, the attenuation component in Eq. (22) becomes

$$\phi = e^{-R_t RT/2P\ L_t/c} \tag{30}$$

where P is the end pressure. The mass flow at the outlet of the tube ($s=L_t$) is

$$\dot{m}_t(L_t,t)=\begin{cases} 0 & \text{if } t<L_t/c \\ e^{-R_t RT/2P\ L_t/c} h\left(t-\dfrac{L_t}{c}\right) & \text{if } t>L_t/c \end{cases} \tag{31}$$

Equation (31) describes in a simple form the mass flow at the tube outlet, for any inlet flow (see Fig. 2). It shows that the flow at the outlet of the tube is attenuated in amplitude and delayed by L_t/c, which represents the time required by the input wave to travel through the entire length of the tube. This solution cannot account for the dependence of the amplitude attenuation on the frequency of the input flow. Its application has to be restricted to relatively small frequencies. The experimental results presented by Hougen et al. [13], showed very small amplitude dependence on frequencies up to 50 Hz, for tubes up to 15 m in length. Considering the fact that Eq. (31) is applied to the valve-cylinder connecting tubes, these limitations are considered more than satisfactory for regular applications.

The tube resistance R_t can be obtained from the expression for the pressure drop along the tube (see Munson et al. [18])

$$\Delta p = f\frac{L_t}{D}\frac{\rho u^2}{2} = R_t u L_t \tag{32}$$

where f is the friction factor, and D the inner diameter of the tube. For fully developed laminar flow $f=64/\mathrm{Re}$, where Re is the Reynolds number. The tube resistance becomes

$$R_t = \frac{32\mu}{D^2} \tag{33}$$

where μ is the dynamic viscosity of air. This result is also derived in Schuder and Binder [12]. Extending the analysis for *wholly turbulent flow* in smooth tubes (the plastic tubes used in this work can be considered smooth), the friction factor can be computed using the *Blasius formula* (Munson et al. [18]),

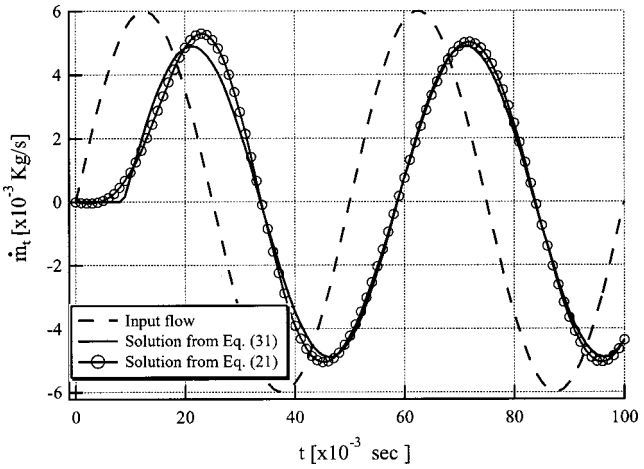

Fig. 3 Tube outlet flow for a sinusoidal flow input

$$f = \frac{0.316}{Re^{1/4}} \tag{34}$$

The tube resistance for wholly turbulent flow becomes,

$$R_t = 0.158\frac{\mu}{D^2}Re^{3/4} \tag{35}$$

In order to use Eq. (31) one has to evaluate the Reynolds number from the input flow values, and compute R_t using Eq. (33) or (35) accordingly.

We compared the results given by Eq. (31) with those obtained by numerical integration of Eq. (21), for a plastic tube with 3.2 mm internal diameter and 3 m length. The input flow was considered to be sinusoidal, with 6×10^{-3} Kg/s amplitude and 30 Hz frequency (see Fig. 3). One can observe from the figure that the simplified equation can effectively predict time delay and the amplitude attenuation.

2.4 Valve Model. The pneumatic valve is a critical component of the actuator system. It is the command element, and should be able to provide fast and precisely controlled air flows through the actuator chambers. There are many available designs for pneumatic valves, which differ in geometry of the active orifice, type of the flow regulating element, number of paths and ports, actuation type, etc. We restricted our study to proportional spool valves, actuated by voice coils. This design presents several advantages: quasi-linear flow characteristic, small time constant, small internal leakage, ability to adjust both chamber pressures using one control signal, very low hysteresis, and low internal friction. In addition, there are many commercially available quality valves. We used a PositioneX, four-way, proportional valve produced by Numatics Inc. The valve features a lapped spool-sleeve assembly, with very low friction. The spool is balanced with respect to the pressure and positioned at the equilibrium (closed) position using two coil springs. This design permits fast

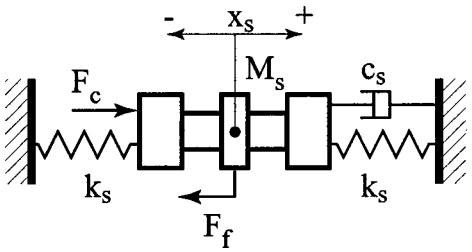

Fig. 4 Valve spool dynamic equilibrium

and precise adjustments of the valve orifice area, providing accurate flow control. If the spool is displaced in the positive direction, one chamber will be connected to the pressure tank through the supply path, and the compressed air will flow inward ($\dot{m}_{in}>0$, $\dot{m}_{out}\approx 0$). The other chamber will be opened to the atmosphere through the exhaust path, and the air will flow outward ($\dot{m}_{in}\approx 0$, $\dot{m}_{out}>0$).

Now we present a model that is developed for the PositioneX valve. This analysis, however, can be easily tailored to model any commercially available pneumatic proportional spool valve. Modeling of the valve involves two aspects: the dynamics of the valve spool, and the mass flow through the valve's variable orifice. Analyzing Fig. 4, the equation of motion for the valve spool can be written as

$$M_s\ddot{x}_s=-c_s\dot{x}_s-F_f+k_s(x_{so}-x_s)-k_s(x_{so}+x_s)F_c \qquad (36)$$

where x_s is the spool displacement, x_{so} is the spring compression at the equilibrium position, M_s is the spool and coil assembly mass, c_s is the viscous friction coefficient, F_f is the Coulomb friction force, k_s is the spool springs constant, and F_c is the force produced by the coil. Simplifying the spring force expressions yields

$$M_s\ddot{x}_s+c_s\dot{x}_s+F_f+2k_sx_s=F_c \qquad (37)$$

The friction force F_f, can be neglected because it is customary in control applications to apply dither signal to the coil, with small magnitude and frequency close to the bandwidth of the valve. The spool will slightly vibrate around the equilibrium position, and the Coulomb friction force will be greatly reduced. Using the force-current expression for the coil and neglecting F_f, Eq. (37) becomes

$$M_s\ddot{x}_s+c_s\dot{x}_s+2k_sx_s=K_{fc}i_c \qquad (38)$$

where K_{fc} is the coil force coefficient, and i_c is the coil current.

The pressure drop across the valve orifice is usually large, and the flow has to be treated as compressible and turbulent. If the upstream to downstream pressure ratio is larger than a critical value P_{cr}, the flow will attain sonic velocity (choked flow) and will depend linearly on the upstream pressure. If the pressure ratio is smaller than P_{cr} the mass flow depends nonlinearly on both pressures. The standard equation for the mass flow through an orifice of area A_v is (see Ben-Dov and Salcudean [8])

$$\dot{m}_v=\begin{cases} C_fA_vC_1\dfrac{P_u}{\sqrt{T}} & \text{if } \dfrac{P_d}{P_u}\leqslant P_{cr} \\ C_fA_vC_2\dfrac{P_u}{\sqrt{T}}\left(\dfrac{P_d}{P_u}\right)^{1/k}\sqrt{1-\left(\dfrac{P_d}{P_u}\right)^{(k-1)/k}} & \text{if } \dfrac{P_d}{P_u}>P_{cr} \end{cases} \qquad (39)$$

where $\dot{m}_v$ is the mass flow through valve orifice, C_f is a nondimensional, discharge coefficient, P_u is the upstream pressure, P_d is the downstream pressure and

$$C_1=\sqrt{\frac{k}{R}\left(\frac{2}{k+1}\right)^{k+1/k-1}}\quad;\quad C_2=\sqrt{\frac{2k}{R(k-1)}};$$
$$P_{cr}=\left(\frac{2}{k+1}\right)^{k/k-1} \qquad (40)$$

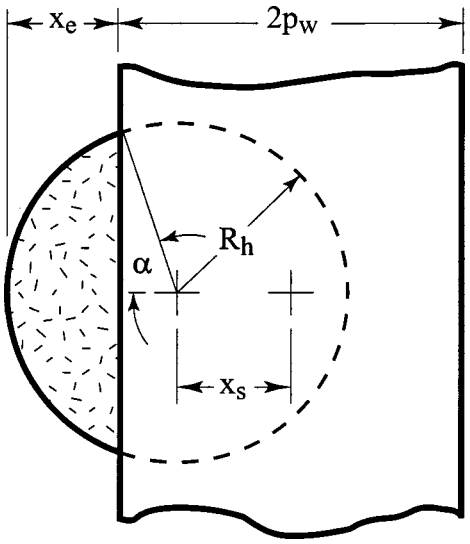

Fig. 5 Orifice area versus spool position

are constants for a given fluid. For air ($k=1.4$) we have $C_1=0.040418$, $C_2=0.156174$, and $P_{cr}=0.528$. Same expression can be used for the leakage flow between the chambers, with the valve area replaced by an experimentally determined leakage area, and the upstream and downstream pressures as the ones from the chambers.

The area of the valve is given by the spool position relative to the radial holes in the valve sleeve, as it is shown in Fig. 5. The area of the segment of the circle delimited by the edge of the spool can be expressed as

$$A_e=2\int_0^{x_e}\sqrt{R_h^2-(\xi-R_h)^2}\,d\xi=2\int_0^{x_e}\sqrt{\xi(2R_h-\xi)}\,d\xi \qquad (41)$$

where A_e is the effective area for one radial sleeve hole, x_e is the effective displacement of the valve spool, and R_h is the hole radius. Integrating Eq. (41) and considering all active holes for an air path in the sleeve (n_h), the effective area of one path in the valve is

$$A_v=n_h\left[2R_h^2\arctan\left(\sqrt{\frac{x_e}{2R_h-x_e}}\right)-(R_h-x_e)\sqrt{x_e(2R_h-x_e)}\right] \qquad (42)$$

The spool width ($2p_w$) is slightly larger than the radius of the hole, to ensure that the air paths are closed even in the presence of small valve misalignments. Thus, the effective displacement of the valve spool x_e will be different from its absolute displacement x_s

$$x_e=x_s-(p_w-R_h) \qquad (43)$$

Substituting Eq. (43) in (42) the valve effective areas for input and exhaust paths becomes

$$A_{v_{in}}=\begin{cases} 0 & \text{if } x_s\leqslant p_w-R_h \\ n_h\left[2R_h^2\arctan\left(\sqrt{\dfrac{R_h-p_w+x_s}{R_h+p_w-x_s}}\right)-(p_w-x_s)\sqrt{R_h^2-(p_w-x_s)^2}\right] & \text{if } p_w-R_h<x_s<p_w+R_h \\ \pi n_hR_h^2 & \text{if } x_s\geqslant p_w+R_h \end{cases} \qquad (44)$$

and,

$$A_{v_{ex}}=\begin{cases}\pi n_h R_h^2 & \text{if } x_s \leq -p_w - R_h \\ n_h\left[2R_h^2 \arctan\left(\sqrt{\dfrac{R_h-p_w+|x_s|}{R_h+p_w-|x_s|}}\right)-(p_w-|x_s|)\sqrt{R_h^2-(p_w-|x_s|)^2}\right] & \text{if } -p_w-R_h<x_s<R_h-p_w \\ 0 & \text{if } x_s \geq R_h-p_w\end{cases} \tag{45}$$

Valve areas for input and exhaust paths versus the spool displacement are presented in Fig. 6. The direction of flows in cylinder chambers have opposite signs, when one chamber is charged the other one is discharged, thus the role of the curves should be switched for the second chamber.

Substituting Eqs. (44) and (45) into Eq. (39) we obtain the expressions for the input and output valve flows.

3 System Identification

The mathematical model of the pneumatic system derived in the previous sections includes a number of geometric and functional characteristics or parameters. Accurate values of these parameters are required in order to use the model in practical applications. Some parameters, such as cylinder bore diameter, piston stroke, or the length of the connecting tubes are provided by the manufacturer or they can be easily measured. Other parameters, such as the critical pressure ratio for choked flow, can be calculated using widely accepted formulas and values for the physical constants involved. The parameters that cannot be directly measured or calculated, have to be estimated (identified) using specially designed experiments. The valve discharge coefficient, spool viscous friction coefficient, static and dynamic friction force between the piston and the cylinder bore, and the piston viscous friction coefficient are parameters of the model that have to be identified experimentally.

An important factor in the pressure differential equation is the mass flow, which can be controlled using the pneumatic valve. Thus, we initiate the system identification process by considering the command element (valve). The value for the coil force coefficient is provided in the valve user manual ($K_{fc}=2.78$ N/A), and M_s and k_s can be easily measured by dismantling the spool. With these values known, the steady state value for the spool displacement can be computed for any constant coil current as,

$$x_s=\frac{K_{fc}}{2k_s}i_c \tag{46}$$

Measuring the flow for several coil currents and fitting the theoretical mass flow expression, Eq. (39), to the experimental values as it is shown in Fig. 7, we determined the discharge coefficient as $C_f=0.25$. The last unknown parameter of the valve is the viscous friction coefficient. We determined its value indirectly by analyzing the step response of the input flow in the actuator chamber charging process while keeping the piston in a fixed position. The theoretical flow curve obtained using Eqs. (38), (39), and (14) closely matches the experimental measurements, for $c_s=7.5$ Kg/s (Fig. 8). Using the identified values, we performed an additional test for the valve flow. Figure 9 presents the dependence of the flow on the downstream pressure, with upstream pressure held constant, for both the experimental values and theoretical outcome.

The unknown parameters of the pneumatic cylinder model include Coulomb and viscous friction forces, inactive volumes at stroke ends, and leakage between chambers. If the detailed geometry of the actuator is available, the inactive volume at the stroke ends can be easily computed. Otherwise, they can be measured by positioning the piston at each end of stroke, filling the ports cavities with a liquid (we recommend lubrication oil), and then mea-

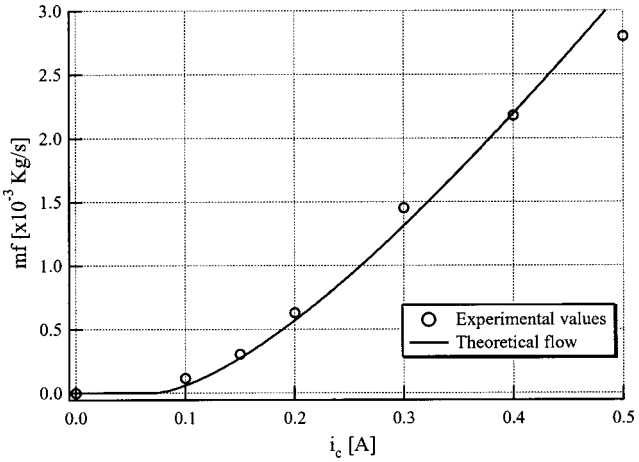

Fig. 7 Valve flow versus coil current

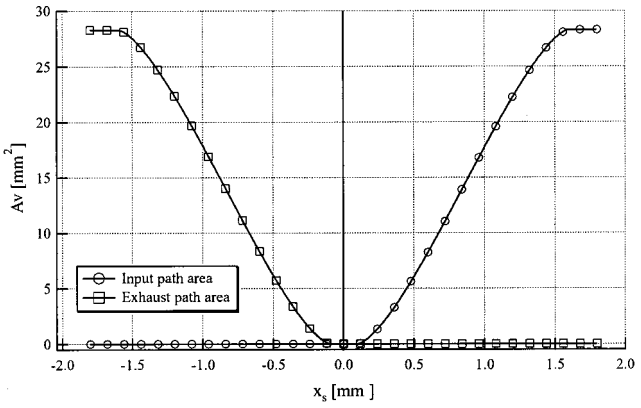

Fig. 6 Input and exhaust valve areas

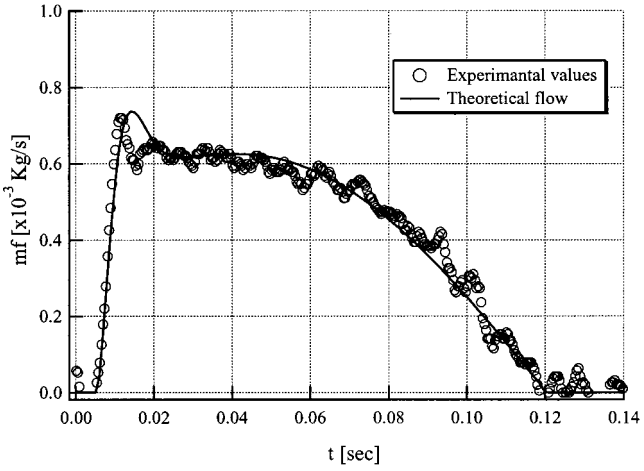

Fig. 8 Valve viscous friction coefficient identification

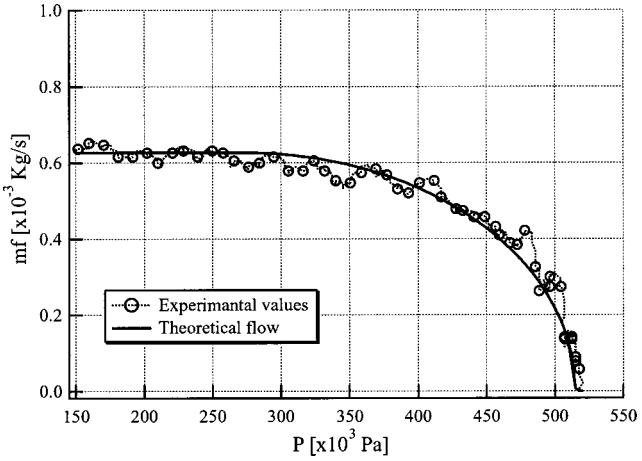

Fig. 9 Valve flow versus downstream pressure

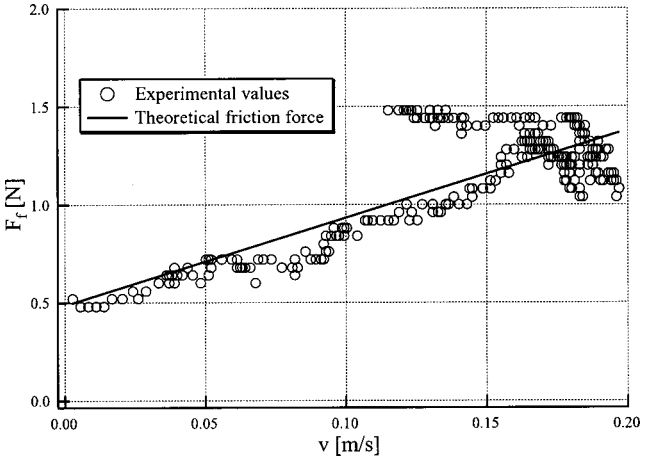

Fig. 11 Dynamic and viscous friction force versus piston velocity, for Numatics 0750D02-03A

suring the volume of the used liquid. The friction forces and the leakage between chambers can only be determined experimentally for each type of cylinder used in a specific application. We considered two types of cylinders, with similar geometric characteristics. First, 0750D02-03A, produced by Numatics, Inc. is a double acting, .75 in. bore diameter, 3 in. stroke pneumatic actuator, with regular rubber piston seals. The second, E16 D 3.0 N Airpel, is produced by Airpot Corp., with .627 in. bore size and 3 in. stroke, and has glass liner cylinder and graphite piston for ultra-low friction.

The Coulomb friction force can be expressed as

$$F_f=\begin{cases} F_{sf} & \text{if } \dot{x}=0 \\ F_{df}\text{sign}(\dot{x}) & \text{if } \dot{x}\neq 0 \end{cases} \tag{47}$$

where F_{sf} and F_{df} are the static and dynamic friction forces, and

$$\text{sign}(x)=\begin{cases} - & \text{if } \dot{x}\leqslant -1 \\ 0 & \text{if } \dot{x}=0 \\ 1 & \text{if } \dot{x}\geqslant 1 \end{cases} \tag{48}$$

In order to determine the friction force we performed a simple experiment. With the piston at rest and air ports disconnected, we applied an increasing force at the rod end. Then the classical Coulomb analysis was used to estimate the static and dynamic friction coefficients. Figure 10 shows the total resistance force for the Numatics actuator, and the corresponding position and velocity of the piston. The static friction is identified from the curve peak as $F_{sf}=3.8$ N. If we neglect the inertia of the piston, in the time interval 0.15–0.40 s, the resistant force can be expressed as

$$F_{rf}=F_{df}\text{sign}(\dot{x})+\beta\dot{x} \tag{49}$$

Plotting the resistance force versus piston velocity, and fitting Eq. (49) to the experimental values (see Fig. 11), we separated the

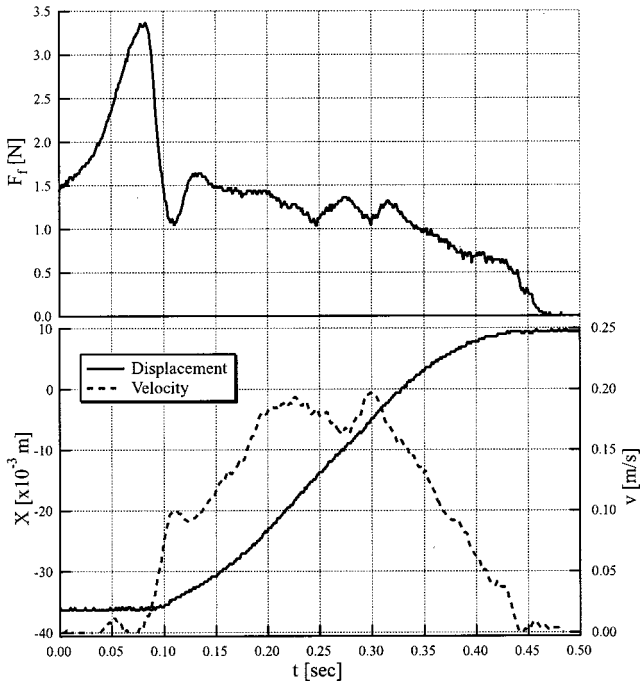

Fig. 10 Numatics 0750D02-03A cylinder friction force

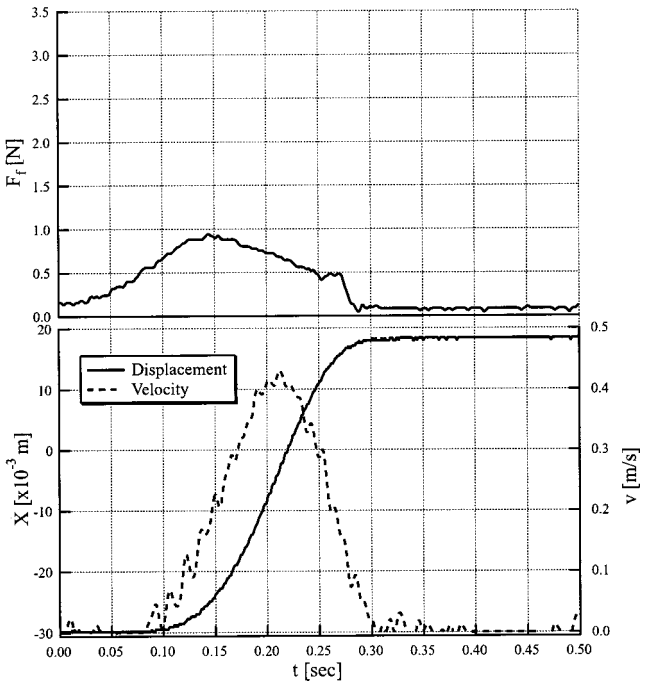

Fig. 12 Airpel E16 D 3.0 N cylinder resistance force

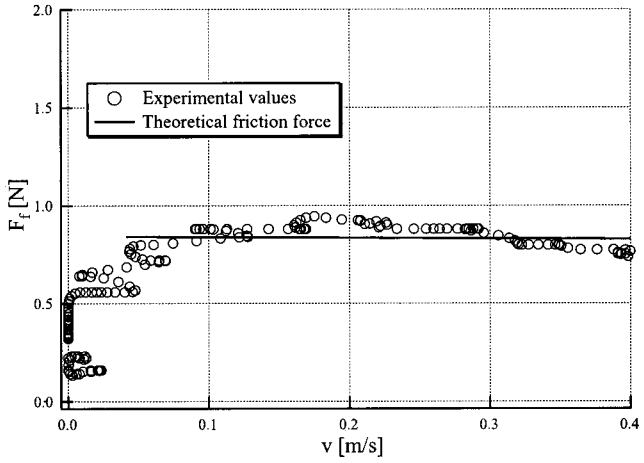

Fig. 13 Cylinder friction force versus piston velocity, for Airpel E16 D 3.0 N

dynamic friction force F_{df} from the viscous friction. We obtained $F_{df}=0.486$ N, and $\beta=4.47$ Kg/s. Figure 12 shows the results of the same experiment performed with the Airpel actuator, and Fig. 13 shows the total resistance force versus velocity. The experiments show no static friction peak, and relative independence of the friction force on the velocity after compensation for piston inertia. The dynamic friction force was identified as $F_d=0.8$ N.

For the Airpel actuator, the leakage between chambers was also measured, and no significant values detected.

4 Experimental Validation of the Model

The complete mathematical model for the pneumatic actuator system consists of the valve dynamics equation, two equations for the chamber pressure time derivatives, and the piston-load equation of motion. The chamber pressure rate of change described by Eq. (16), has to be customized for the two cylinder chambers using the corresponding input and exhaust flows, and the corresponding upstream and downstream pressures for the charging or discharging process. The valve flows through the input and output paths can be written as

$$\dot{m}_{v_{\text{in}}}=C_f A_{v_{\text{in}}}\frac{P_s}{\sqrt{T}}\dot{m}_r(P_s,P) \tag{50}$$

$$\dot{m}_{v_{\text{ex}}}=C_f A_{v_{\text{ex}}}\frac{P_i}{\sqrt{T}}\dot{m}_r(P_s,P_a) \tag{51}$$

where P_i, $i=1,2$ is the absolute pressure in the corresponding cylinder chamber, and,

$$\dot{m}_r=\begin{cases} C_1 & \text{if } \dfrac{P_d}{P_u}\leqslant P_{cr} \\ C_2\left(\dfrac{P_d}{P_u}\right)^{1/k}\sqrt{1-\left(\dfrac{P_d}{P_u}\right)^{(k-1)/k}} & \text{if } \dfrac{P_d}{P_u}>P_{cr} \end{cases} \tag{52}$$

is the reduced flow function. Using Eq. (31) the flows through the connecting tubes become,

$$\dot{m}_{t_{\text{in}}}=\phi_{\text{in}}\dot{m}_{v_{\text{in}}}(t-\tau) \tag{53}$$

$$\dot{m}_{t_{\text{ex}}}=\phi_{\text{ex}}\dot{m}_{v_{\text{ex}}}(t-\tau) \tag{54}$$

where ϕ_{in} and ϕ_{ex} are the flow attenuations from Eq. (30), and τ is the tube time delay. Substituting these equations in Eq. (16) we obtain the final equations for chambers pressure as,

$$\dot{P}_1=\frac{C_f R\sqrt{T}}{V_{01}+A_1\left(\frac{1}{2}L+x\right)}[\alpha_{\text{in}}\phi_{\text{in}}\overline{A}_{v1_{\text{in}}}P_s\dot{m}_r(P_s,\overline{P}_1) - \alpha_{\text{ex}}\phi_{\text{ex}}\overline{A}_{v1_{\text{ex}}}\overline{P}_1\dot{m}_r(\overline{P}_1,P_a)]-\alpha\frac{P_1A_1}{V_{01}+A_1\left(\frac{1}{2}L+x\right)}\dot{x} \tag{55}$$

$$\dot{P}_2=\frac{C_f R\sqrt{T}}{V_{02}+A_2\left(\frac{1}{2}L-x\right)}[\alpha_{\text{in}}\phi_{\text{in}}\overline{A}_{v2_{\text{in}}}P_s\dot{m}_r(P_s,\overline{P}_2) - \alpha_{\text{ex}}\phi_{\text{ex}}\overline{A}_{v2_{\text{ex}}}\overline{P}_2\dot{m}_r(\overline{P}_2,P_a)]-\alpha\frac{P_2A_2}{V_{02}+A_2\left(\frac{1}{2}L-x\right)}\dot{x} \tag{56}$$

where the variables with overbars represent values delayed by time τ. These equations, together with Eqs. (1) and (38), completely describe the pneumatic system. They include the effect of the external load, piston friction, the difference in the effective areas on the two sides of the piston on the actuator force output, the different heat transfer characteristics at charging or discharging process and compression-expansion of air due to piston motion, the flow attenuation and delay due to the tubes, nonlinear compressible flow through the valve, and the valve dynamics. They can be numerically solved for any valve command i_c, and can be used as a mathematical model for control design.

Two sets of experiments were conducted in order to verify the proposed mathematical model. In the first experiment we measured the pressures in both cylinder chambers, and the force provided by the actuator using absolute pressure piezoelectric transducers, and a strain gage force cell. The piston was fixed at the middle of the stroke, and a step input of 0.5 A has been applied to the valve coil (see Fig. 14). Two length of connecting tubes were used: 0.5 m and 2 m. Figures 15 and 16 show both numerical and experimental results for actuator chamber pressures and output force, corresponding to the valve step input of 0.5 A, and for both tube lengths. There is a close agreement between the theoretical and experimental curves, with very good amplitude match and less than 0.001 seconds time shift. Both figures show a significant time delay between the valve command and corresponding pressure or force output, due to the connecting tubes and the valve dynamics. The additional 0.005 sec time delay for the 2 m tube case matches the theoretically computed value. The attenuation of

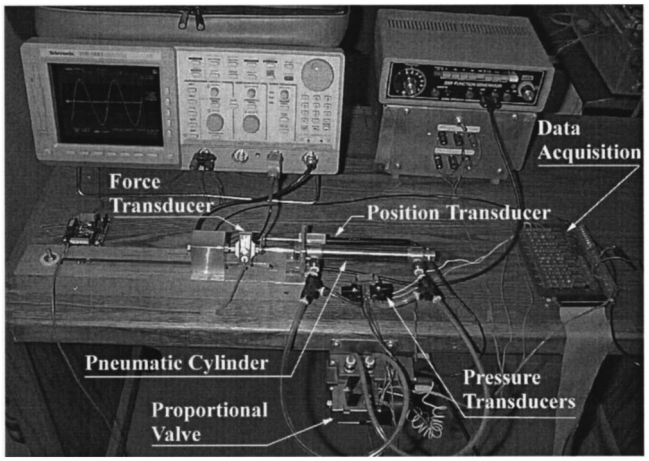

Fig. 14 The experimental setup

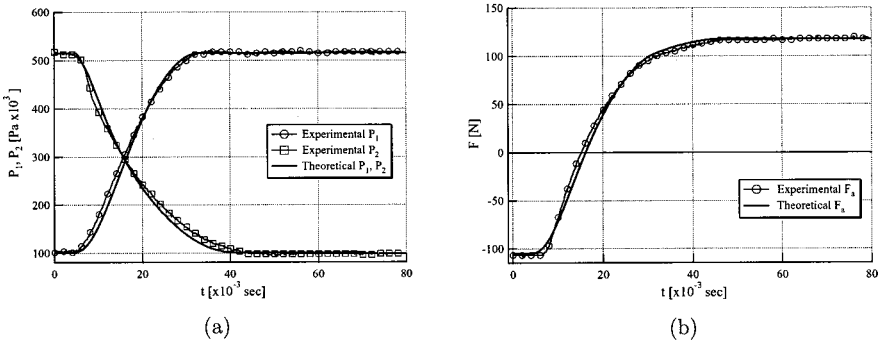

Fig. 15 Numerical and experimental actuator pressures (*a*) and force (*b*) for 0.5 A step coil current and 0.5 m tube length

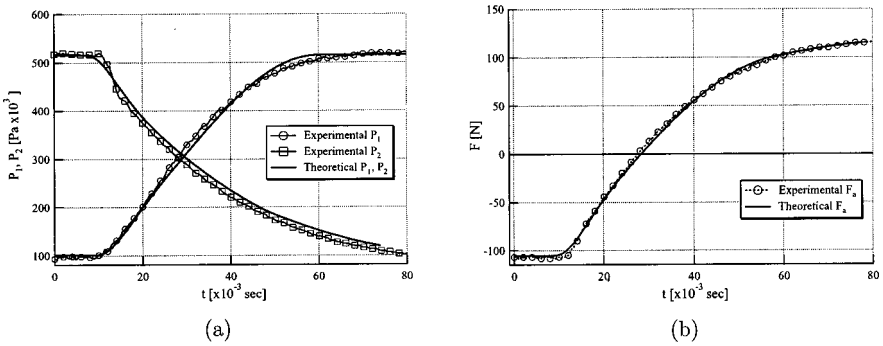

Fig. 16 Numerical and experimental actuator pressures (*a*) and force (*b*) for 0.5 A step coil current and 2 m tube length

the mass flow amplitude induced by the tube is reflected by the significantly larger (more than double) time duration required to reach the maximum value of the output force, when the long tubes are used. In the second experiment a sinusoidal command current was applied to the valve coil and the piston motion was recorded. The experiments were conducted without applying any external load to the piston rod. Figures 17 and 18 show the experimental and numerically simulated results for the Numatics 0750D02-03A and Airpel E16 D 3.0 N pneumatic cylinders. In both cases the agreement between the outcome of the experiment and the theoretical model is excellent.

5 Conclusions

In this article we developed a detailed mathematical model for a dual action pneumatic actuator controlled by a proportional, coil actuated valve. The proposed model is not only accurate, but also

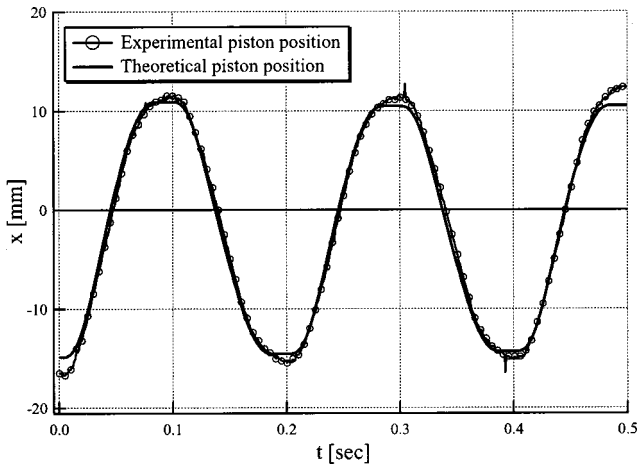

Fig. 17 Experimental and numerical piston position for 1.5 V and 5 Hz sinusoidal valve current for Numatics 0750D02-03A cylinder

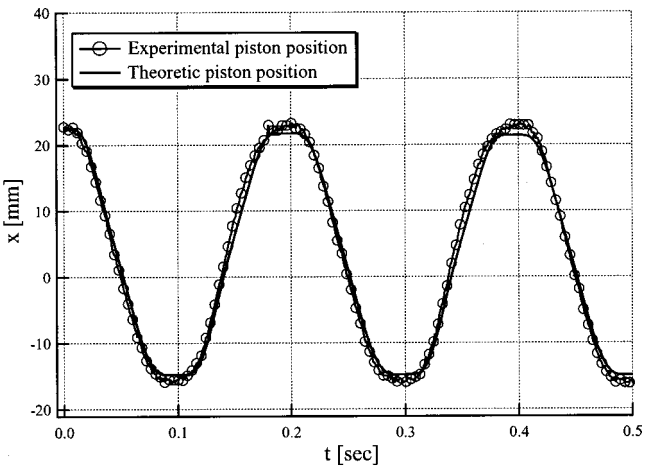

Fig. 18 Experimental and numerical piston position for 1.5 V and 5 Hz sinusoidal valve current for Airpel E16 D 3.0 N cylinder

sufficiently simple such that it can be used online in control applications. Specifically, one can use the model to develop high performance force controller for applications in robotics and automation. We developed a pneumatic cylinder model that includes the piston seals friction, the difference in effective areas on the opposite sides of the piston, the inactive volumes at the ends of the stroke and the connecting ports, and the difference in the heat transfer characteristics for the charging and discharging processes of the cylinder chambers. We introduced a new equation to account for the influence of the tubes that connect the pneumatic cylinder with the valve. Explicit formulas were derived for the tube resistance for laminar and turbulent flow. Valve dynamics, the nonlinearity of the valve effective area with respect to the coil current, and the nonlinear turbulent flow through the valve orifice were also considered. The results obtained by numerical simulation were compared with the experimental data, and excellent agreement was found.

References

[1] Shearer, J. E., 1956, ''Study of Pneumatic Process in the Continuous Control of Motion with Compressed Air-I, II,'' Trans. ASME, Feb., pp. 233–249.

[2] Burrows, C. R., and Webb, C. R., 1966, ''Use of the Root Loci in Design of Pneumatic Servo-Motors,'' Control, Aug., pp. 423–427.

[3] Liu, S., and Bobrow, J. E., 1988, ''An Analysis of a Pneumatic Servo System and Its Application to a Computer-Controlled Robot,'' ASME J. Dyn. Syst., Meas., Control, **110**, pp. 228–235.

[4] Bobrow, J. E., and Jabbari, F., 1991, ''Adaptive Pneumatic Force Actuation and Position Control,'' ASME J. Dyn. Syst., Meas., Control, **113**, pp. 267–272.

[5] McDonell, B. W., and Bobrow, J. E., 1993, ''Adaptive Traking Control of an Air Powered Robot Actuator,'' ASME J. Dyn. Syst., Meas., Control, **115**, pp. 427–433.

[6] Arun, P. K., Mishra, J. K., and Radke, M. G., 1994, ''Reduced Order Sliding Mode Control for Pneumatic Actuator,'' IEEE Trans. Control Syst. Technol., **2**, No. 3, pp. 271–276.

[7] Tang, J., and Walker, G., 1995, ''Variable Structure Control of a Pneumatic Actuator,'' Trans. ASME J. Dyn. Syst. Meas., **117**, pp. 88–92.

[8] Ben-Dov, D., and Salcudean, S. E., 1995, ''A Force-Controlled Pneumatic Actuator,'' IEEE Trans. Rob. Autom., **11**, No. 6, pp. 906–911.

[9] Richard, E., and Scavarda, S., 1996, ''Comparison Between Linear and Nonlinear Control of an Electropneumatic Servodrive,'' ASME J. Dyn. Syst., Meas., Control, **118**, pp. 245–118.

[10] Al-Ibrahim, A. M., and Otis, D. R., 1992, ''Transient Air Temperature and Pressure Measurements During the Charging and Discharging Processes of an Actuating Pneumatic Cylinder,'' *Proceedings of the 45th National Conference on Fluid Power*.

[11] Hullender, D. A., and Woods, R. L., 1985, ''Modeling of Fluid Control Components,'' *Proceedings of the First Conference on Fluid Control and Measurement*, FLUCOME '85, Pergamon Press, Tokyo, London.

[12] Schuder, C. B., and Binder, R. C., 1959, ''The Response of Pneumatic Transmission Lines to Step Inputs,'' ASME J. Basic Eng., **81**, pp. 578–584.

[13] Hougen, J. O., Martin, O. R., and Walsh, R. A., 1963, ''Dynamics of Pneumatic Transmission Lines,'' Energy Convers. Manage., **35**, No. 1, pp. 61–77.

[14] Andersen, B., 1967, *The Analysis and Design of Pneumatic Systems*, Wiley, New York.

[15] Whitmore, S. A., Lindsey, W. T., Curry, R. E., and Gilyard, G. B., 1990, ''Experimental Characterization of the Effects of Pneumatic Tubing on Unsteady Pressure Measurements,'' NASA Technical Memorandum 4171, pp. 1–26.

[16] Elmadbouly, E. E., and Abdulsadek, N. M., 1994, ''Modeling, Simulation and Sensitivity Analysis of a Straight Pneumatic Pipeline,'' Energy Convers. Manage., **35**, No. 1, pp. 61–77.

[17] Chester, C. R., 1971, *Techniques in Partial Differential Equations*, McGraw-Hill, New York.

[18] Munson, B. R., Young, D. F., and Okiishi, T. H., 1990, *Fundamentals of Fluid Mechanics*, Wiley, New York.